Articles

Backbone Dynamics of Green Fluorescent Protein and the Effect of Histidine 148 Substitution†

Markus H. J. Seifert,*,‡,§ Julia Georgescu,‡ Dorota Ksiazek,‡ Pawel Smialowski,‡ Till Rehm,‡ Boris Steipe,|| and Tad A. Holak*,‡

Max-Planck-Institute for Biochemistry, 82152 Martinsried, Germany, and Department of Biochemistry, University of Toronto, Toronto, Ontario, Canada

Received July 19, 2002; Revised Manuscript Received November 27, 2002

ABSTRACT: Green fluorescent protein (GFP) and its mutants have become valuable tools in molecular biology. GFP has been regarded as a very stable and rigid protein with the β-barrel shielding the chromophore from the solvent. Here, we report the ^{15}N nuclear magnetic resonance (NMR) studies on the green fluorescent protein (GFPuv) and its mutant His148Gly. ^{15}N NMR relaxation studies of GFPuv show that most of the β-barrel of GFP is rigid on the picosecond to nanosecond time scale. For several regions, including the first α-helix and β-sheets 3, 7, 8, and 10, increased hydrogen−deuterium exchange rates suggest a substantial conformational flexibility on the microsecond to millisecond time scales. Mutation of residue 148 located in β-sheet 7 is known to have a strong impact on the fluorescence properties of GFPs. UV absorption and fluorescence spectra in combination with ^{1}H−^{15}N NMR spectra indicate that the His148Gly mutation not only reduces the absorption of the anionic chromophore state but also affects the conformational stability, leading to the appearance of doubled backbone amide resonances for a number of residues. This suggests the presence of two conformations in slow exchange on the NMR time scale in this mutant.

Green fluorescent proteins not only provide powerful tools for monitoring gene expression, protein movement, and protein interactions (*1*, *2*) but also exhibit complex photophysical behavior in both the ensemble (*3*−*5*) and single-molecule measurements (*6*−*8*). GFP[1] was first discovered in the jellyfish *Aequorea victoria* which shows spots of green light along the margin of its umbrella upon electrical or mechanical stimulation (*9*). This light is produced by the interaction of the light-emitting protein aequorin and GFP; the latter shifts the light emission in the living organism from blue to green (*10*−*12*). The optical absorption, fluorescence, and ultrafast dynamic fluorescence properties of GFP are commonly explained by a three-state model (*3*, *4*, *13*): the chromophore exists in either a neutral (A) or an anionic state, which occurs in a thermodynamically unstable intermediate form (I) and a stable form (B). Fluorescence dynamics are rationalized by the model of an intramolecular Förster cycle (*14*) between the states, i.e., A → A* → I* → I → A, where the asterisks indicate excited states. Upon illumination of GFP with UV light, an A → B photoconversion takes place that reduces the absorbance of state A and increases the absorbance of state B (*15*, *16*).

Until now, the family of GFP-like proteins comprised 27 cloned and spectroscopically characterized proteins (*17*), and high-resolution crystal structures of 18 are available. The overall structure of GFP consists of an 11-stranded β-barrel with a central helix that carries the chromophore (*18*, *19*). The X-ray diffraction studies and a variety of physicochemical methods highlight an apparent exceptional low conformational flexibility of the GFP fold which preserves the planar chromophore structure. Low *b* factors (*19*) of the tyrosine 66 side chain indicate a rigid chromophore conformation (*20*), which is an important prerequisite for a high quantum yield of fluorescence. At room temperature, denatured GFP or model chromophores in solution show no

† This work was supported by Grant SFB 533 from Deutsche Forschungsgemeinschaft (German Research Foundation).

* To whom correspondence should be addressed. M.H.J.S.: e-mail, markus.seifert@4sc.com; phone, +49-89-7007-630. T.A.H.: e-mail, holak@biochem.mpg.de; phone, +49-89-8578-2673.

‡ Max-Planck-Institute for Biochemistry.

§ Present address: 4SC AG, 82152 Martinsried, Germany.

|| University of Toronto.

[1] Abbreviations: asCP, *Anemonia sulcata* chromoprotein (asFP595); GFP, *A. victoria* green fluorescent protein; CFP, cyan fluorescent protein; YFP, yellow fluorescent protein; CSA, chemical shift anisotropy; DsRed, *Discosoma striata* red fluorescent protein; NMR, nuclear magnetic resonance; $\Delta\nu$, NMR line width; CBCA(CO)NH, $^{13}C_\beta-^{13}C_\alpha-(^{13}C')-^{15}N-^{1}H_N$ correlation; *f*, NOE enhancement factor; H−D exchange, hydrogen−deuterium exchange; HNCA, $^{1}H_N-^{15}N-^{13}C_\alpha$ correlation; HNCO, $^{1}H_N-^{15}N-^{13}C'$ correlation; HSQC, heteronuclear single-quantum coherence; {I}−S NOE, nuclear Overhauser effect on nucleus S by saturating nucleus I; $J(\omega)$, spectral density of rotational diffusion; *n*, number of β-sheets in a β-barrel; T_1, longitudinal relaxation time; T_2, transversal relaxation time; TROSY, transverse relaxation-optimized spectroscopy; R_1, longitudinal relaxation rate; R_2, transversal relaxation rate; *S*, shear number in β-barrels; τ_C, overall rotational correlation time; τ_m, mixing time; $\Delta\sigma$, anisotropy of the chemical shift tensor; η, cross-correlation rate of ^{15}N-labeled CSA and ^{1}H−^{15}N dipolar relaxation; ω, Larmor frequency.

10.1021/bi026481b CCC: $25.00
Published on Web 02/14/2003

significant fluorescence due to a high conformational flexibility of the chromophore moiety (*21*, *22*). However, when frozen in an ethanol glass at 77 K, such model compounds become highly fluorescent (*23*). Inside the protein environment the chromophore is very sensitive to mutations of surrounding residues that alter the permitted degrees of freedom of the chromophore (*24*). Structural rigidity in combination with the high melting temperature of *Aequorea* GFP [78 °C (*23*)] and the stability of the GFP fold against denaturants and proteases lead to the view of GFP being a very stable and conformationally inflexible protein (*2*, *23*).

However, recent ^{19}F NMR studies of the cyan variant of GFP conducted in our laboratory indicated conformational flexibility in or near the chromophore moiety with His148 being most likely involved in this process (*25*). In contrast to many spectroscopic techniques, NMR spectroscopy provides a large frequency range for studying dynamical processes at atomic resolutions from picosecond to second time scales and even longer. For example, motional and thermodynamical information for backbone amides in proteins can be obtained from measurements of ^{15}N relaxation rates in ^{15}N-labeled proteins (*26*, *27*). Hydrogen−deuterium exchange experiments allow characterization of conformational fluctuations in secondary structure elements (*28*). NMR has been suggested as a tool for elucidating the dynamics of chromophore formation, water accessibility of the chromophore, and conformational flexibility in GFP (*13*, *29*), but NMR studies on GFPs turned out to be a challenge due to the strong tendency of GFPs to aggregate (*25*).

This study investigates the dynamical properties of the GFP β-barrel that plays an essential role in protecting the chromophore from environmental influences. We present the characterization of the backbone molecular motions of GFPuv [also known as the cycle 3 mutant of wild-type GFP (*30*, *31*)] by ^{15}N NMR relaxation measurements, which allowed for the determination of the residue specific spectral densities of motions on the picosecond to nanosecond time scale. We also describe hydrogen−deuterium exchange experiments. The state of aggregation was investigated by NMR measurements of translational diffusion. To identify residues that may play a role in the integrity of the β-barrel, sequences of several GFP variants and the perlecan-binding G2 fragment of nidogen-1 (*32*) are compared using the structure specific and sequence specific alignments.

It has been shown previously that the fluorescence properties of not only GFP (*24*, *33*) but also red fluorescent variant DsRed and the chromoprotein asCP (*34*) are very sensitive to mutations of residues corresponding to His148 and Thr203 in GFP, which are supposed to play a major role not only in proton transfer during the intramolecular Förster cycle but also in protein folding and chromophore maturation. For example, in asCP mutations at position 148 with amino acids other than serine, cysteine, asparagines, or glycine result in ill-folded or colorless proteins (*34*). To investigate the influence of histidine 148 on backbone dynamics, the His148Gly mutation was introduced in GFPuv. ^{1}H−^{15}N NMR correlation spectra show the presence of a second conformation in the mutant protein.

EXPERIMENTAL PROCEDURES

Sequence Alignment. The FSSP/DALI database [http://www.ebi.ac.uk/dali/ (*35*)] was used to align the sequence of GFP [PDB entry 1ema (*18*)], GFPuv [also known as the cycle 3 mutant (Phe99Ser, Met153Thr, and Val163Ala); PDB entry 1b9c (*30*, *31*)], DsRed [PDB entry 1ggx (*36*)], and the perlecan-binding G2 fragment of nidogen-1 [PDB entry 1h4u (*32*)]. The sequence of asCP was aligned according to ref *34*.

Sample Preparation. Samples of GFPuv labeled with ^{15}N, ^{15}N and ^{2}H (99%), ^{15}N and ^{13}C, or ^{15}N, ^{13}C, and ^{2}H (70%) were produced as described in refs *37* and *38*. The samples were dissolved in phosphate-buffered saline (PBS) at pH 7.0.

To produce the GFPuv His148Gly mutant, the QuikChange site-directed mutagenesis kit was used for the His148Gly point mutation. Mutagenesis primers were designed to introduce the specific experimental mutation (MWG-DNA). After PCR, products were digested (37 °C, 1 h) with the *Dpn*I restriction enzyme (10 units/L) and transformed into *Epicurian coli* XL1_Blue supercompetent cells. Transformation plates were incubated at 37 °C for 16 h. DNAs from eight different colonies were sequenced, and seven of them had the desired mutation. After this, His148Gly GFPuv was expressed in *Escherichia coli*. Expression was controlled by the T7 promotor and provided by the gene for β-lactamase. After induction with 0.5 mM isopropyl thiogalactoside (IPTG) six-His-tagged GFP was overexpressed in BL21-(DE3) cells in 1 L of LB medium for 6 h at 37 °C. The cell pellet was resuspended in 50 mL of lysis buffer [300 mM NaCl and 50 mM Na_2HPO_4 (pH 8)] with 1 mg of DNAse, 1 mg of RNAse, 1 mg of $MgCl_2$, and 0.1 M phenylmethanesulfonyl fluoride (PMSF) and then sonicated with Micro-Tip and centrifugated for 45 min at 80 000 rpm in a Beckmann centrifuge. The protein was purified by Ni^{2+} affinity chromatography. Ni−NTA resin (Qiagen) was incubated with the supernatant for 1 h at 4 °C, poured into a column, and subsequently washed with 100 mL of lysis buffer. The protein was eluted from the Ni−NTA resin with 20 mL of elution buffer [300 mM NaCl, 50 mM Na_2HPO_4, and 500 mM imidazole (pH 8.0)]. Then the protein was dialyzed against PBS [115 mM NaCl, 8 mM KH_2PO_4, and 16 mM Na_2HPO_4 (pH 7.0)]. GFPuv His148Gly was concentrated to 15−20 mg/mL using a Centricon 10 instrument (Millipore). After additional gel filtration with a Superdex 75 column (Pharmacia), the sample was concentrated again to a concentration of 20−25 mg/mL. The purity of the sample was checked by mass spectroscopy. Two independent samples were produced to ensure the reproducibility of the effects observed by NMR spectroscopy.

Optical Spectroscopy. UV absorption spectra of 10 μM GFPuv and GFPuv His148Gly in PBS buffer were recorded on a Perkin-Elmer UV−vis spectrophotometer at room temperature. The spectra were scaled using a known molar extinction coefficient of GFP (ϵ_M = 21 000 M^{-1} cm^{-1} at a λ of 277 nm). Optical excitation and emission spectra were measured on a Perkin-Elmer LS50B spectrometer at 25 °C. The protein concentration was adjusted to 50 nM. To acquire the excitation spectra, the emission at 510 nm was measured. To record the emission spectra, the samples were excited at 396 nm. In both cases, a slit of 2.5 nm was used.

NMR Spectroscopy. All heteronuclear ^{1}H−^{15}N NMR experiments were performed on either a Bruker DRX500, DRX600, or DMX750 spectrometer equipped with 5 mm ^{1}H, ^{13}C, and ^{15}N triple-resonance TXI probe heads, including triple-axis gradients (DRX600 and DMX750) or a *z*-axis gradient (DRX500). The spectra were recorded at 310 K with

a sweep width of 17.5 ppm for ^{1}H and 42 ppm for ^{15}N.

Assignment of the backbone resonances was achieved with triple-resonance spectra, including HNCA (*39*), TROSY-HNCA (*40*), HN(CO)CA, HNCO, CBCA(CO)NH (*39*) spectra; a HBHA(CBCACO)NH (*39*) spectrum was also recorded on a Bruker Cryoprobe DRX 600 spectrometer. In addition, HSQC (*41*) spectra of selectively ^{15}N-labeled Gly, Phe, Tyr, Met, Ala, Leu, Lys, Ile, and Val and inversely ^{15}N-labeled Asn, Thr, His, and Asp samples of GFPuv were recorded. Two-dimensional (2D) NOESY (τ_m = 160 ms) spectra and three-dimensional (3D) NOESY-HSQC (τ_m = 160 ms) spectra supplemented the NMR data. Where appropriate, the spectra were recorded on 70 or 99% deuterated samples of GFPuv. The program Sparky (*42*) and in-house software CCNMR (*43*) were used for analyzing the spectra. Details of NMR data acquisition and resonance assignment are described in refs *37* and *38*.

A pH titration and a H−D exchange (*28*) experiment were conducted on the basis of ^{1}H−^{15}N HSQC spectra (*41*). For the titration, the pH of a ^{15}N-labeled sample of GFPuv in PBS buffer was reduced from pH 7.7 to 6.1 in steps of 0.1 by adding the appropriate amount of 1 M H_3PO_4. For each step, a HSQC spectrum was recorded. For the H−D exchange experiment, the ^{15}N-labeled sample of GFPuv was lyophilized and dissolved in 99.99% D_2O. Then a series of 16 HSQC spectra was recorded. The measurement time for one spectrum was 1 h. In the following month, one spectrum per week was recorded. Finally spectra after 2, 3, and 5 months were recorded. The protein was stored at 4 °C between measurements.

NMR Diffusion Measurements. The translational diffusion coefficient (*44*) of GFPuv at 310 K was measured by a modified Watergate ^{1}H one-dimensional (1D) sequence (*45*) with strong, sine-shaped gradients centered on the selective Watergate pulse. The gradients were calibrated by 1D NMR imaging of a 3.5 mm Teflon plug in a standard 5 mm NMR tube filled with $CuSO_4$-doped water. The I/I_0 signal attenuation due to translational diffusion is given by

$$I = I_0 e^{-bD}$$

with D being the translational diffusion coefficient. The corresponding b value for sine-shaped gradients was calculated using the relationship (*46*)

$$b = \gamma^2 G^2 \frac{\delta^2}{\pi^2}(4\Delta - \delta)$$

where G represents the maximum strength of the gradient. The timing of the gradients before and after the selective Watergate pulse was set to 17 ms (Δ) and 15 ms (δ). The apparent mass of the protein can be calculated from the diffusion coefficient according to (*47*)

$$M = \left(\frac{kT}{6\pi\nu FD}\right)^3 \frac{4\pi N_A}{3(\bar{V}_2 + \kappa\bar{V}_1)}$$

For the apparent mass calculation, the following parameters (T = 310 K) were used: protein form factor F (1.03), hydration of the protein κ (0.34), viscosity of water ν (6.91 × 10^{-4} Ns/m^2), specific volume of the protein $\bar{V}_2$ (0.731 × 10^{-3} m^3/kg), and specific volume of water $\bar{V}_1$ (1.00669 × 10^{-3} m^3/kg). k and N_A represent the Boltzmann constant and Avogadro's number, respectively.

NMR Relaxation Measurements. For investigation of the backbone flexibility, the relaxation parameters T_1 (*48*) and T_2 (*49*), the heteronuclear ^{1}H−^{15}N Overhauser effect (*50*), and the ^{1}H−^{15}N dipolar−^{15}N CSA cross-correlation rate (*51*) were measured as described in the corresponding references. The measurements were performed on the ^{15}N-labeled sample, as well as on the ^{15}N- and ^{2}H (99%)-labeled samples of GFPuv, at proton frequencies of 500 and 600 MHz. In the heteronuclear ^{1}H−^{15}N Overhauser experiment, saturation of the amide protons was achieved by application of 120° pulses prior to the experiment (*52*). NOE values were given by the ratios of peak heights in the experiments with and without proton saturation. Water suppression during the T_2, NOE, and CSA relaxation experiments was achieved by using the Watergate 3-9-19 or improved Watergate 5 pulses (*45*). The relaxation delays used for determination of the T_1 relaxation times were 12.4, 260.4, 508.4, 756.4, and 1004.4 ms and for T_2 relaxation times 20.8, 41.6, 124.8, and 166.4 ms. In the T_1 experiment, water saturation was avoided by using low-power water-flip-back pulses. The recycle delay (T_R) was set to 1.5 s. The T_1 measurement was conducted according to the method described in ref *53*. Therefore, a nonoptimal recycle delay ($T_R < 2T_1$) merely reduces the sensitivity of the T_1 experiment without introducing systematic errors (*53*). The experimental peak intensities of the T_1 and T_2 experiment were fitted to the equation $A \exp(-t/T_x)$ (x = 1 or 2) with a Levenberg−Marquardt algorithm using the Sparky relaxation extension. The statistical errors of curve fitting were determined by Monte Carlo simulation. In the CSA experiment, the cross-correlation rate η was calculated using the relationship $I_A/I_B = \tanh(2\Delta\eta)$ with I_A and I_B being the peak intensities resulting from the two experiments described in ref *51* and the delay Δ being set to 22 ms. The measurement error was derived from the signal-to-noise ratio of the corresponding peaks.

Reduced Spectral Density Mapping. Amide relaxation was analyzed assuming contributions only from dipolar coupling between nitrogen and its attached proton and from the ^{15}N chemical shift anisotropy (*54*). The spectral density function $J(\omega)$ has quite small values when $\omega = \omega_H$ (*55*−*57*), which leads to the assumption that it varies only little in the vicinity of ω_H. When $\omega = \omega_H \pm \omega_N$, we used the approximation $J(\omega)$ = const or $J(\omega) \propto 1/\omega$. Values of $J(\omega)$ can thus be calculated at $\omega = 0$, ω_N, and $0.870\omega_H$ from T_1, T_2, and NOE data. Both approximations resulted in almost identical values for the spectral density function for these frequencies. This agreement proves the applicability of the approximation used, as these two methods give lower and upper bounds for the exact values of the spectral density function. An isotropic overall correlation time of rotational diffusion τ_c was then determined from the T_1/T_2 ratio of residues that showed little internal motion and no significant exchange broadening [NOE > 0.6, T_1/T_2 ratio within one standard deviation of the mean value (*58*)]. It is possible to calculate τ_c analytically, assuming that the contributions of the spectral density function at the proton frequencies can be neglected [$J(\omega_H) = J(\omega_H + \omega_N) = J(\omega_H - \omega_N) = 0$] as proposed by Fushman et al. (*59*):

$$\tau_c = (2\omega_N)^{-1}\sqrt{(6T_1/T_2 - 7)}$$

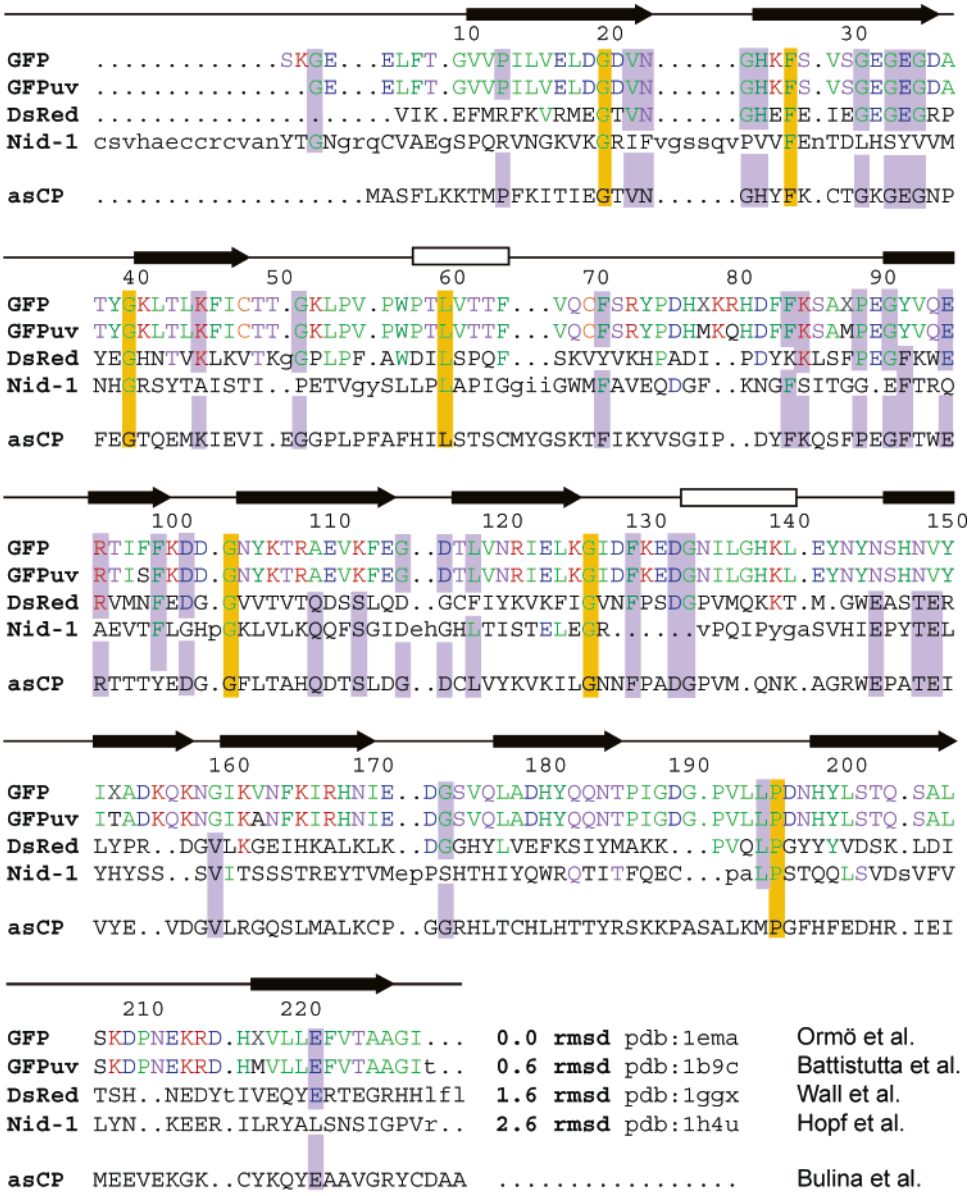

FIGURE 1: Sequence alignment of GFP (PDB entry 1ema), GFPuv (PDB entry 1b9c), DsRed (PDB entry 1ggx), nidogen-1 (PDB entry 1h4u), and asCP (no structural data available). The alignment of GFP, GFPuv, DsRed, and nidogen-1 is based on a FSSP/DALI database search (*35*). The sequence of asCP was aligned according to ref *34*. The backbone rmsd values are given in angstroms. The amino acids conserved in all five proteins are marked with yellow bars. Blue bars highlight amino acids conserved to a smaller degree.

Several recent studies of spectral density mapping showed that this assumption is valid for residues that exhibit little internal motion (*55*, *56*). The errors in the values of the spectral density were calculated from the experimental errors of the relaxation rates by standard error propagation.

RESULTS

Sequence Alignment. As can been seen in Figure 1, *A. victoria* GFP/GFPuv, *Discosoma striata* DsRed, *Anemona sulcata* asCP, and the G2 fragment of mouse nidogen-1 share several conserved amino acids despite their different origins and functions. The low rmsd values for the structures of GFP, DsRed, and nidogen-1 indicate a high degree of structural similarity despite a low degree of sequence homology [e.g., only 10% for nidogen-1 in comparison to GFP (*32*)]. Residues Gly20, Phe27, Gly40, Leu60, Gly104, Gly127, and Pro196 (GFP numbering) are conserved in all the proteins that are being considered. Most of these similarities correlate well with the start or end of secondary structure elements, suggesting a key role especially for the conserved glycine residues for the overall GFP fold. In addition, Phe71 in GFP, nidogen-1, and asCP is changed to a tyrosine in DsRed. Phe100 in GFP, DsRed, and nidogen-1 is mutated to tyrosine in asCP. His148 in GFP is changed into a tyrosine in nidogen-1. Furthermore, several residues are conserved among DsRed, nidogen-1, and asCP, including Gln110, Ser113, Phe92, Glu146, Thr149, Glu150, and Val160. Figure 2 shows a stereoplot of the GFP crystal structure highlighting the residues conserved in all the proteins.

Translational Diffusion. Panels A and B of Figure 3 depict the result of the translational diffusion NMR experiment. A diffusion constant D of (120 $\pm$ 10) μm^2/s was measured, considering the uncertainties of the gradient calibration. Using the specific model given in Experimental Procedures, this results in an apparent mass for GFPuv of 45 $\pm$ 10 kDa under the conditions used in NMR experiments. This is

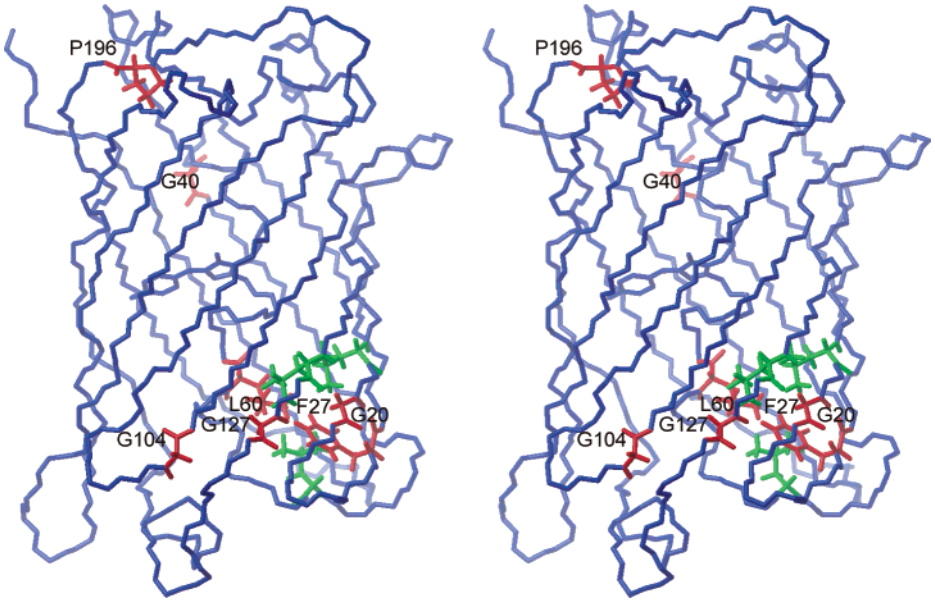

FIGURE 2: Stereoplot of the crystal structure of GFPuv (PDB entry 1b9c) with the residues conserved in GFP, DsRed, asCP, and the G3 fragment of nidogen-1 depicted in red. Residues L18, L53, and L125 that form the hydrophobic pocket with L60 and F27 are shown in green. This figure was created using MOLMOL (*80*).

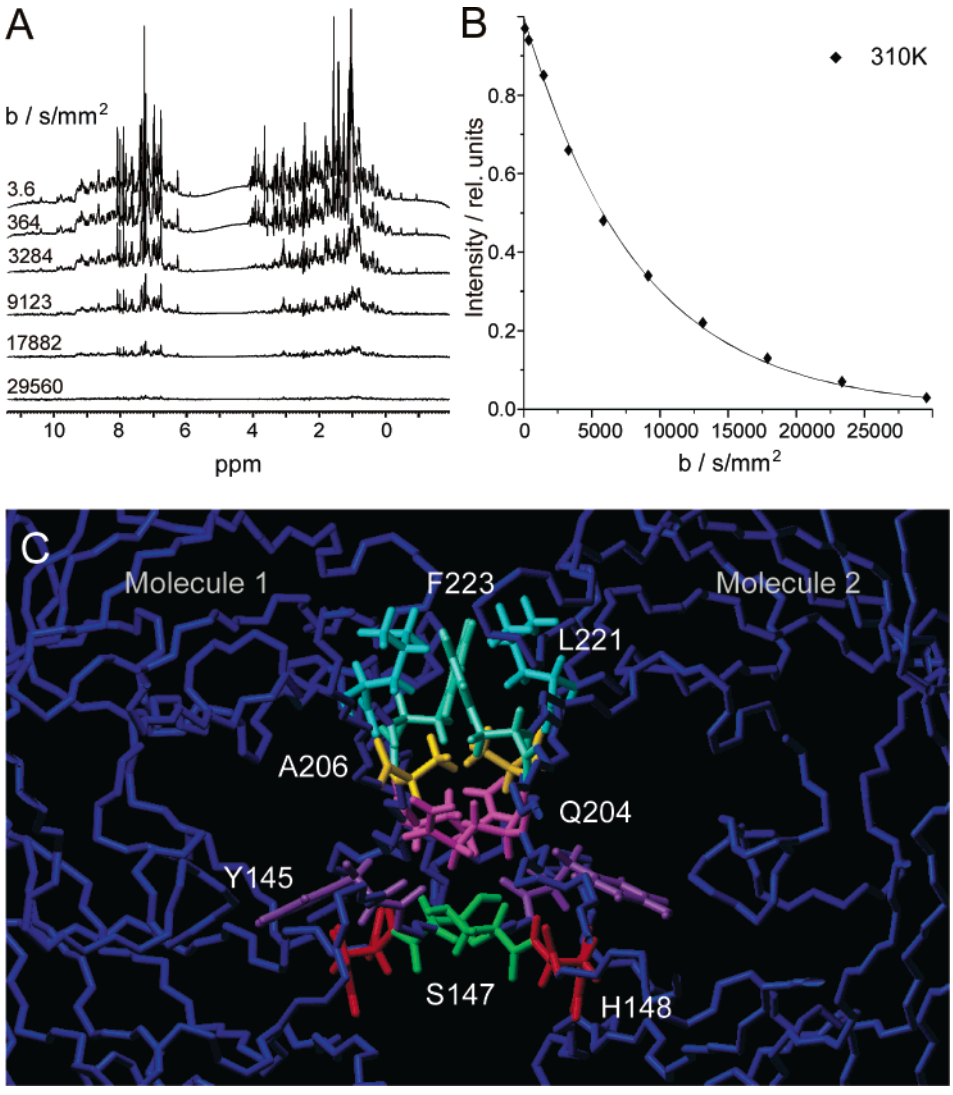

FIGURE 3: (A and B) NMR measurement of the translational diffusion of GFPuv and (C) the dimerization interface of GFP.

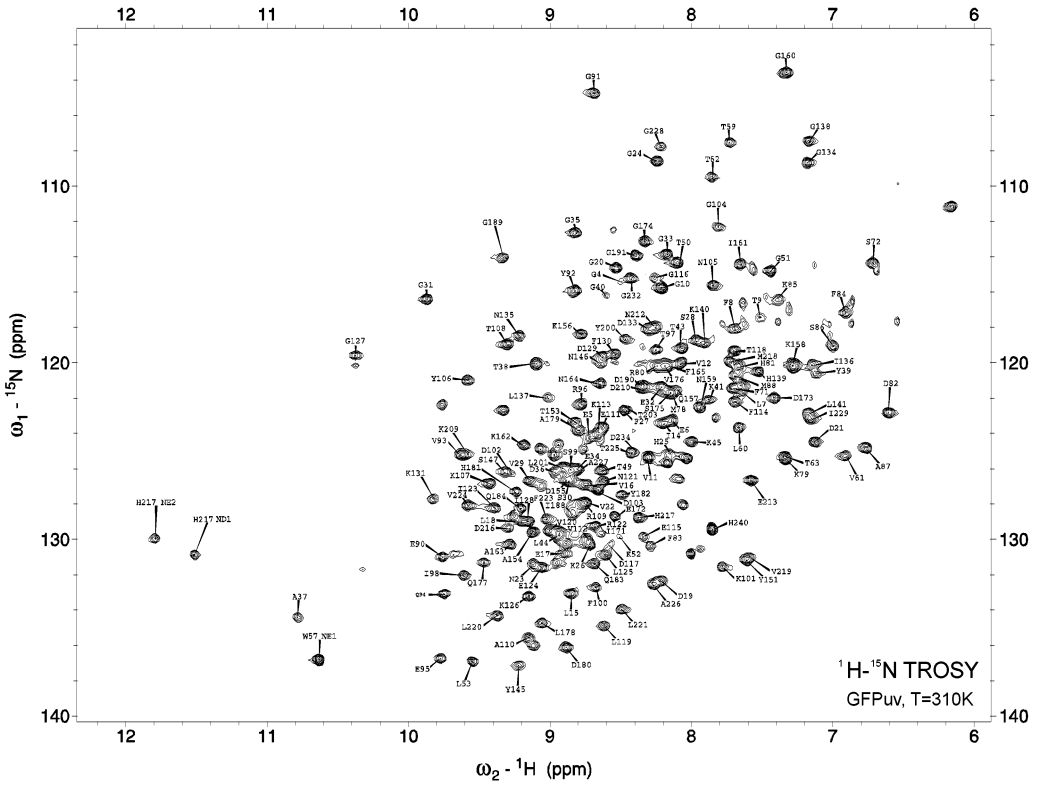

FIGURE 4: 2D ^{1}H−^{15}N NMR TROSY spectrum of GFPuv at 310 K. The labels indicate the sequence specific resonance assignment.

significantly larger than the value of 27 kDa for the monomeric GFPuv, but still smaller than the value of 54 kDa expected for a dimer, suggesting that GFPuv in solution exists as a mixture of monomers and dimers. This is in agreement with the known dimer dissociation constant K_D of 0.1 mM of GFPs as determined by analytical ultracentrifugation (*60*). Figure 3C illustrates the GFP dimer interface as observed by X-ray crystallography.

NMR Assignment. Eighty percent of the backbone amide groups of GFPuv were assigned by standard triple-resonance methods (see Figure 4). The assignment was complicated by a substantial amount of missing interresidue connectivity in the triple-resonance NMR spectra. The assignment of the central α-helix and of β-sheets 7, 8, and 10 could not be completed. These difficulties can be explained by the necessity of a neutral pH, the tendency of GFP to aggregate in solution, and the presence of conformational exchange on microsecond to millisecond time scales, as described below, that lead to line broadening.

NMR Relaxation. All samples showed essentially the same relaxation behavior. The results of the measurements at 500 and 600 MHz agreed within the expected scaling of the R_1, R_2, and hetNOE values with the magnetic field strength. Figure 5 summarizes the results of the relaxation measurements on ^{15}N- and ^{2}H (99%)-labeled GFPuv at 600 MHz. The longitudinal relaxation rate R_1 is 0.5 s^{-1} on average with only the N- and C-terminus showing higher rates of up to 1.0 s^{-1}. The average transversal relaxation rate R_2 is 27 s^{-1} with lower values mainly for the C-terminal residues. The ^{1}H−^{15}N heteronuclear NOE values cluster around 0.8, indicating the absence of pronounced motions on the picosecond to nanosecond time scale for nearly all the residues except the C-terminal ones which exhibit negative NOE values. The ^{1}H−^{15}N dipolar−^{15}N CSA cross-correlation rate η is 15 s^{-1} on average with lower values at the C-terminus of the protein. The overall rotational correlation time of GFPuv (τ_c) was estimated to be 22 ns by calculation of the R_1/R_2 ratios for the backbone nitrogen of residues located in structured parts of the protein (hetNOE > 0.6).

Reduced Spectral Density Mapping. Figure 6 shows the results of the relaxation data analysis with the reduced spectral density mapping, the pH sensitivity, and the H−D exchange rate of the amide protons. Most of the backbone nitrogens show no significant differences in spectral densities $J(\omega)$ except those located in the termini of the protein. A decrease in $J(0)$ in combination with an increase in $J(\omega_N)$ and $J(0.87\omega_H)$ is an indication of higher flexibility of the corresponding nitrogen atom. Only the first residues of β-sheet 1 and residues Phe84, Gln94, Glu111, Gly116, and Asn146 exhibit spectral densities that point to a flexibility higher than those of the average protein backbone. Residues Phe84, Gly116, and Asn146 are located in the loops that connect β-strands of the β-barrel, which explains their higher flexibility. Residues 94 and 111 are located in β-strands 4 and 5. Therefore, the reduced spectral density mapping clearly shows that GFPuv has a rigid structure on the nanosecond to picosecond time scale with only the termini and a small number of backbone amides having increased flexibility. The low values of η/R_2 at the beginning of the first α-helix and the first β-sheet indicate a flexibility on the microsecond time scale higher than that of the average protein residues (*61*). Analysis of the relaxation data according to the Lipari−Szabo model (*62*) failed because the fitting of the diffusion tensor was not possible. This may be due to the aggregation of GFPuv which leads to monomer and dimer states interconverting fast on the NMR time scale. Since NMR measurements are sensitive only to the ensemble average, the relaxation data also represent values averaged

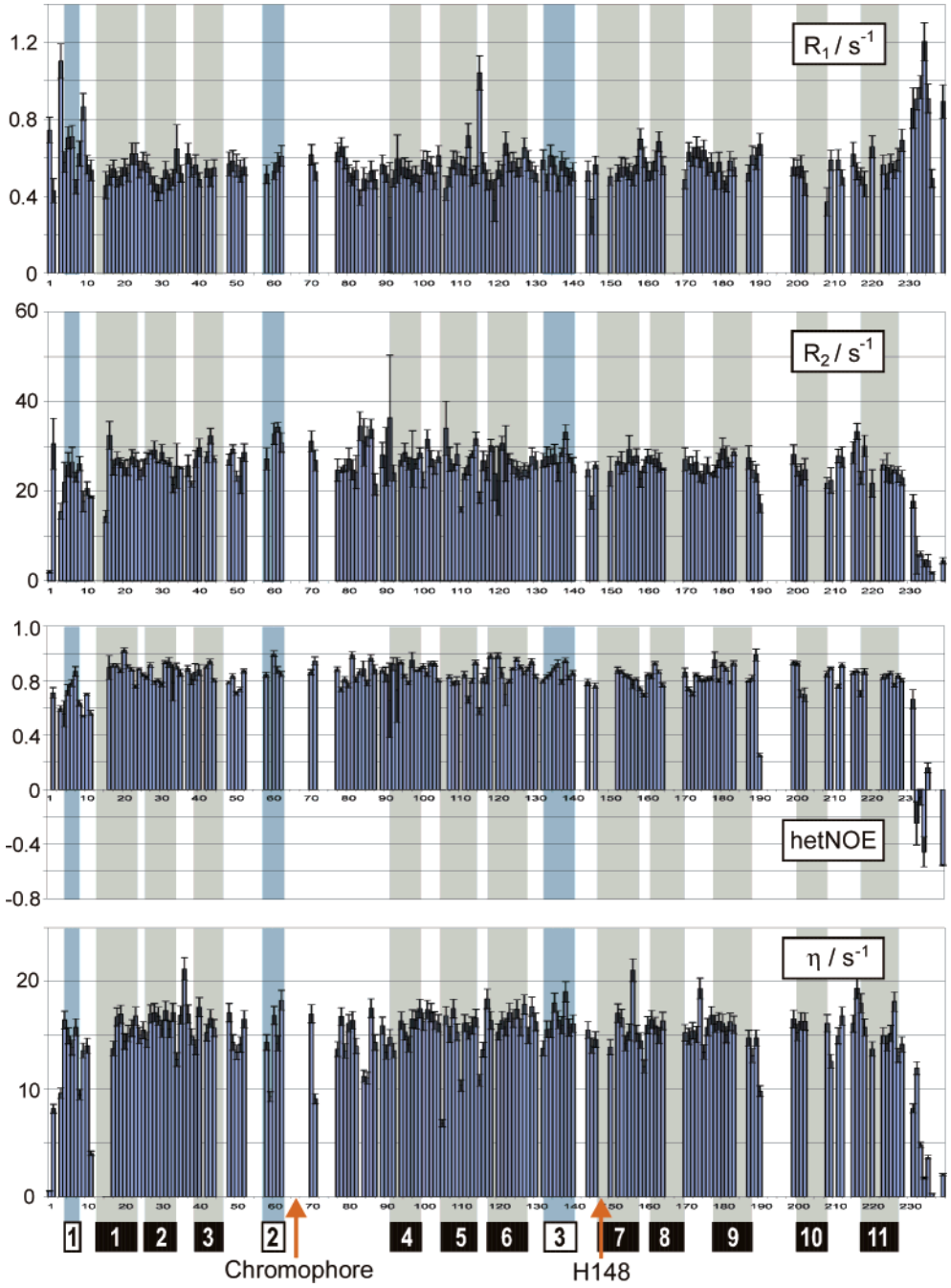

FIGURE 5: Relaxation rates R_1 and R_2, hetNOE values, and η values as a function of the amino acid sequence of GFPuv. Missing bars indicate residues which were not assigned or where no reliable relaxation data could be collected.

over monomer and dimer states. This clearly affects the measured overall correlation time and additionally prevents the fitting of a unique rotational diffusion tensor. However, GFP dimerization does not include any interleaved monomer units (Figure 3C). Therefore, fast internal backbone motions are expected to be unchanged in parts of the protein that are not located in the dimerization interface which allows for the comparison and interpretation of spectral densities of the corresponding amide moieties.

pH Titration and H−D Exchange. pH titration of ^{15}N-labeled GFPuv revealed that the amide chemical shifts of residues Asp21−Lys26, Gly40, Gly104, Gly116, Gly127, Gly134, Leu137−His139, Thr203, Gly228, and Ile229 are sensitive to pH (see Figure 6B and Figure S2 of the Supporting Information). Except for Thr203, Gly134, and Leu137−His139, all of them are located in loops and exposed to solvent. The region of residues 134−139 corresponds to a solvent-exposed α-helical section. Residue Thr203 is one of the residues which are in contact with the chromophore.

The results of the H−D exchange experiment are shown in Figure 6B. The resonances were divided into four categories according to the time scale of H−D exchange: fast (completely exchanged after 15 min), intermediate (significant exchange within 12 h), slow (significant exchange within several days and up to 1 month), and very slow (only little exchange after several months). Figure 6B shows that the central regions of β-strands 1, 3−6, and 11 exhibit slower average H−D exchange than β-strands 2 and 7−10 (see also Figure S3 of the Supporting Information). The β-barrel of

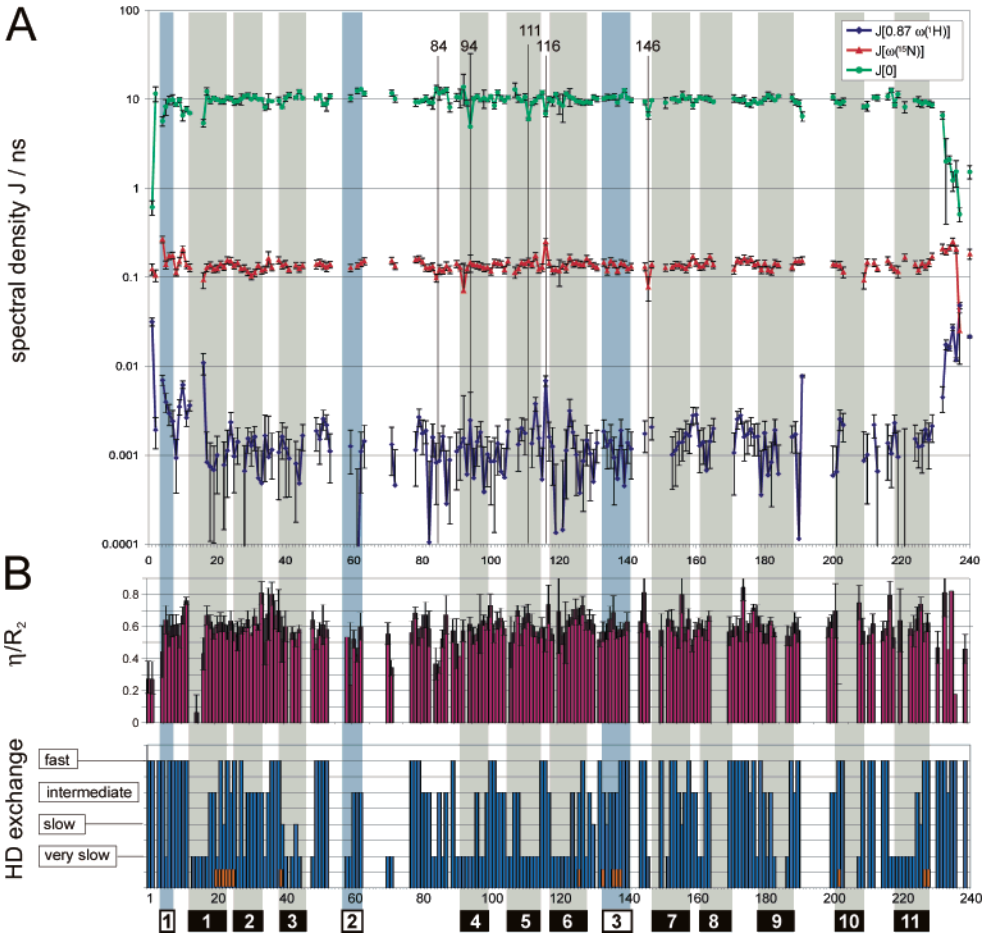

FIGURE 6: Reduced spectral density $J(\omega)$, the R_2/η ratio, H−D exchange rates, and the pH sensitivity of the backbone amide resonances in GFPuv at 310 K. The pH sensitive residues are marked with orange boxes in the diagram of H−D exchange rates. The secondary structure elements of GFPuv are depicted as empty (α-helix) and filled (β-sheet) boxes.

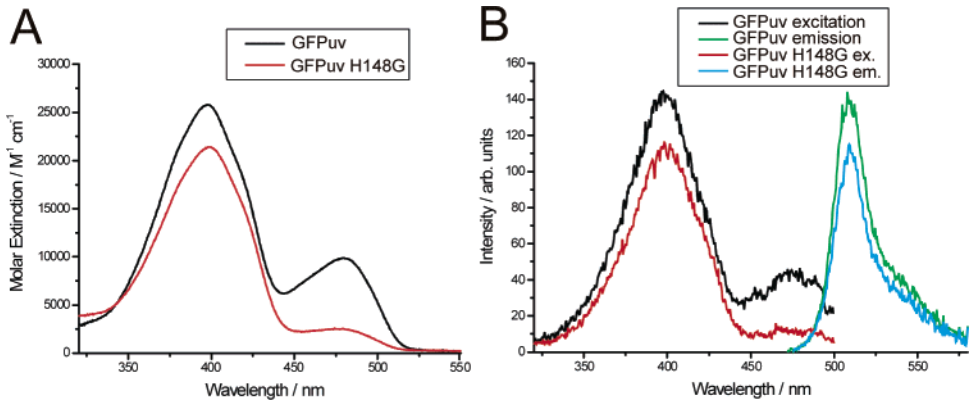

FIGURE 7: UV−vis absorption (A) and excitation and emission spectra (B) of GFPuv and GFPuv mutant H148G.

GFPuv is formed by the following sequence: β-strands 1, 2, 3, 11, 10, 7, 8, 9, 4, 5, and 6. The difference in H−D exchange rates in the β-strands provides indications for more pronounced low-frequency motions on one side of the β-barrel corresponding roughly to β-strands 7−10.

His148Gly Mutant. The UV absorption and excitation spectra of GFPuv and GFPuv mutant His148Gly show that the mutation does not significantly affect the absorption maximum of the chromophore's A state at 398 nm (Figure 7). The intensity of peak A in the absorption spectrum and the emission peak at 508 nm is reduced to 82% in the mutant compared to that in GFPuv. In contrast, peak B in the absorption spectrum is reduced to 26% in the mutant protein. Peaks A and B are usually assigned to the neutral and anionic state of the chromophore, respectively. The emission at 510 nm is reduced to 80% in the mutant protein which is in agreement with the reduced absorption of state A.

The His148Gly mutation leads to the appearance of double peaks for several residues in the HSQC spectrum of GFPuv His148Gly (Figure 8A and Figure S4 of the Supporting Information). The peak volume ratio of minor and major peaks was on average 0.45:1 at 310 K. Minor peaks corresponded to the original resonances in the spectrum of GFPuv. The small difference in chemical shift of major and minor peaks of approximately 30−60 Hz indicates a time scale of exchange on the order of 0.01−0.1 s. At 290 K, the

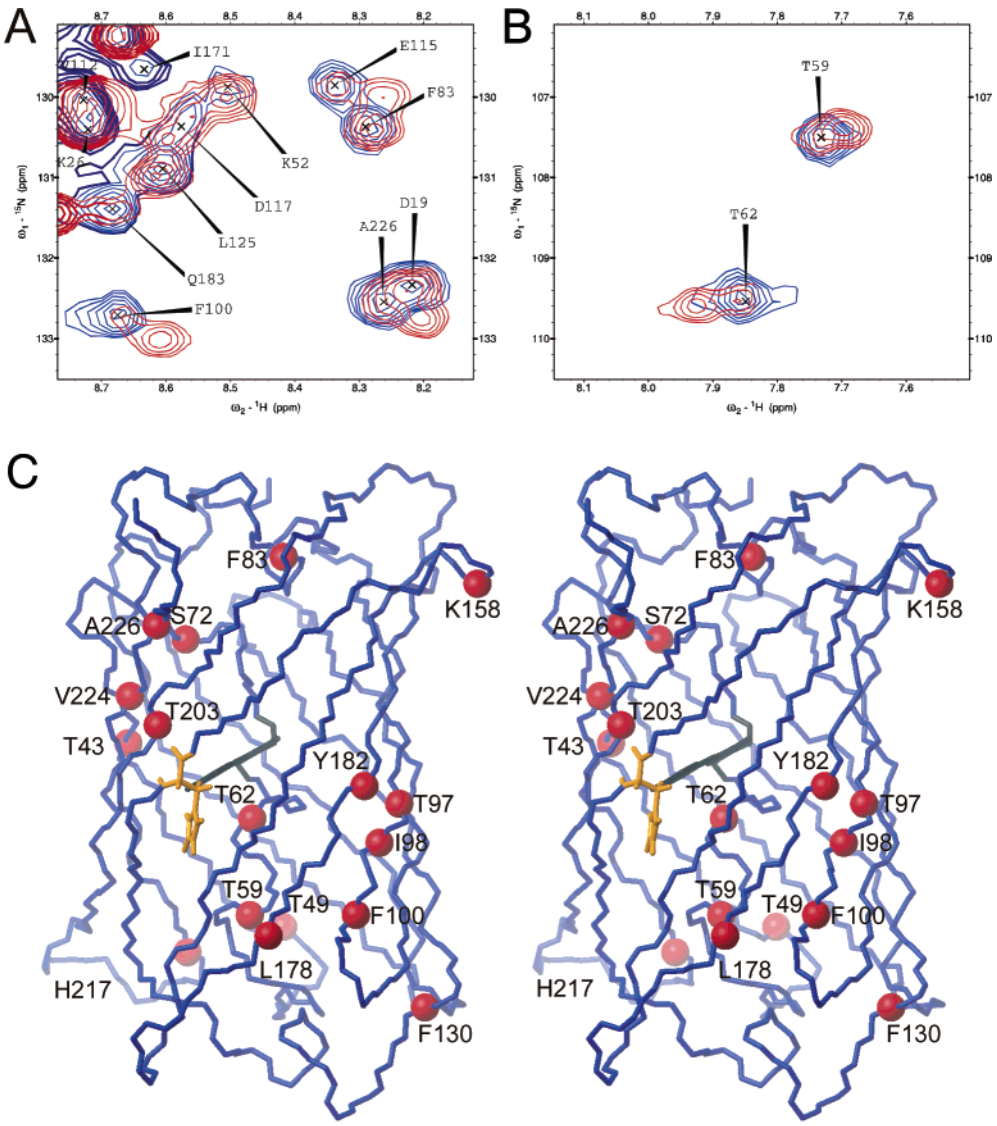

FIGURE 8: Two regions from the $^{1}H-^{15}N$ HSQC spectrum of GFPuv (blue) and GFPuv His148Gly (red) (A and B) exemplifying the appearance of double peaks in the mutant His148Gly for several backbone amide groups. The affected amide nitrogens are shown in panel C as red balls with respect to the GFP structure. The chromophore and H148 are depicted in black and orange, respectively. These structures were drawn using MOLMOL (*80*).

minor peaks seem to be even more pronounced, although broadening of the resonances due to a higher solvent viscosity complicated the detection of several resonances. These temperature-dependent double peaks provide an indication of slow exchange processes affecting the backbone structure of the mutant. The following residues with known assignments are affected by these exchange processes: Thr43, Thr49, Thr59, Thr62, Ser72, Phe83, Thr97, Ile98, Phe100, Phe130, Lys158, Leu178, Tyr182, Gln183, Thr203, His217, Val224, and Ala226. In addition, the heteronuclear NOE values of the minor conformation are significantly reduced for the following residues (data not shown): Gly33, Glu34, Gly40, Lys41, Phe84, Phe100, Gly116, Asn164, and Phe165. The heteronuclear NOE values of the major conformation are comparable to those obtained for GFPuv. Figure 8B maps the location of residues that were assigned and unambiguously affected by exchange on the crystal structure of GFP. These residues cluster in the central α-helix (as far as assigned) and β-strand 4; however, the effect is not limited to residues near His148, and many residues distributed all over the β-barrel are affected.

DISCUSSION

Conserved Residues. Comparison of GFP-like proteins from several organisms is useful in revealing residues that are crucial for GFP stability. Four glycines, one phenylalanine, one leucine, and one proline residue are conserved among all species. The conserved amino acids Phe27 and Leu60 together with Leu125 (Ile in asCP and Phe in Dsred) form a hydrophobic core within the barrel (see Figure 2) that may play a role in positioning the central α-helix during protein folding; in this process, the β-strands have to wrap around the central helix to close the barrel. It is usually assumed that protein folding is driven by the thermodynamic advantage inherent in the sequestration of hydrophobic residues in the interior of the protein away from the solvent (*13*). However, in the core of GFP, i.e., around the chromophore, there is a surprising number of polar residues (*2*). Therefore, other nucleation points for protein folding are

likely to exist. Hydrophobic residues Phe27 and Leu60 are conserved in all proteins mentioned here, suggesting that these residues might be important for the stable protein structure, presumably during the folding process.

In addition, conserved glycine residues may also play an essential role in GFP folding. It has been shown that the Thr22Gly mutation in *Drosophila* drk protein, which restores the otherwise highly conserved glycine residue in the diverging β-turn connecting β-strands 3 and 4 of SH3 domains, significantly stabilizes the drk SH3 structure (*63*). Conserved glycines with a strong correlation to the beginning or end of β-strands have been reported for the large subunit of ribulose bisphosphate carboxylase/oxygenase from *Anacystis nidulans* (*64*). It was proposed that glycines might serve to be hinges enabling the movement of loops. Such hinges may also be important for the GFP β-barrel.

Several other residues are conserved in only three or four of the compared species. On the basis of an alignment of GFP and the nidogen-1 G2 fragment, Hopf et al. (*32*) have speculated that both proteins are derived from a common ancestor. Our alignment, including now additionally DsRed and asCP, corroborates this hypothesis.

Dimerization. The apparent protein mass of GFPuv of approximately 45 kDa determined from translational diffusion indicates the presence of a mixture of monomers (27 kDa) and dimers (54 kDa) in solution. The extent of self-association in the GFPuv sample is obvious when comparing the overall rotational correlation of GFP (238 residues, $\tau_c =$ 22 ns) to that of, for example, maltose binding protein [MBP (*65*), 370 residues, $\tau_c = 16$ ns], which was measured at the same temperature as GFP. It was proposed that the mutations present in GFPuv, Phe99Ser, Met153Thr, and Val163Ala, reduce the aggregation tendency (*66*). Our results clearly show that these mutations cannot prevent self-association of GFPuv under the conditions needed for NMR spectroscopy, i.e., the high protein concentration of approximately 1 mM. Additionally, one-dimensional ^{1}H NMR spectra (see Figure S1 of the Supporting Information) of GFPuv and Clontech EGFP (Phe64Leu and Ser65Thr) show no significant difference in ^{1}H line width between GFPuv and EGFP under these conditions. Additional mutations such as Ala206Lys, Leu221Lys, and Phe223Arg (see ref *67* and Figure 3C) are known to reduce the extent of hydrophobic interaction and might therefore allow for production of NMR samples with less aggregation.

It is not yet clear if these hydrophobic interactions play a physiological role for any kind of membrane association or interaction with the light-emitting protein aequorin. It is known that other GFPs, like *Renilla* GFP, are obligate dimers (*2*), whereas DsRed forms a tetramer (*68*). In general, the self-association of GFPs is a relatively conserved feature. Recently, Campbell et al. (*68*) have speculated that a relationship between oligomerization and habitat temperature may exist. Hydrophobic interactions may also be relevant for the interaction of GFP and the light-emitting protein aequorin. Remarkably, the very structurally similar (2.6 Å rmsd compared to GFP) nidogen-1 is supposed to play a role in membrane assembly (*32*). Therefore, further studies should address the structural and phylogenetic relationship of GFPs to proteins such as nidogen-1 and, for example, β-barrel membrane proteins OmpX, OmpA (*69*), and others (*70*).

Backbone Dynamics. Figure 9 maps experimental findings on the GFP secondary structure. With 80% of the backbone amides being assigned, some important conclusions can be drawn from the relaxation measurements. (i) The overall structure of GFP is rigid on the picosecond to nanosecond time scale. This is in agreement with molecular dynamics simulations which predicted a rms deviation of only 0.9 Å during a 1 ns period (*71*). (ii) A significant variation of the η/R_2 values can be observed in β-sheets 4−6 and especially in the first α-helix, where the η/R_2 values are lower at the beginning and at the end of the sheets than at the center of the sheets. This indicates motions on the microsecond to millisecond time scale in the turns connecting the sheets. These features are not observed on the picosecond to nanosecond time scale in the spectral density function $J(\omega)$ at least for the β-sheets. (iii) One side of the protein, corresponding to β-strands 7−10, shows increased H−D exchange rates. Increased H−D exchange rates in β-sheets are usually attributed to hydrogen bonds being broken by conformational fluctuations on the microsecond to millisecond time scale (*28*). The first two observations may not be unexpected, but the last issue needs further discussion.

In crystal structures of GFPs, a reduced interstrand hydrogen bonding network (see panels A and B of Figure 9) can be observed for β-strands 7, 8, and 10. This may be caused either by dynamic conformational processes or by inefficient side chain packing inside the GFP β-barrel which leads to diverging β-strands and therefore larger interstrand distances. For β-barrel folds, purely geometrical considerations showed that efficient side chain packing and low conformational energies are related to the overall geometry of the cylinder which is characterized by the number of β-sheets n and the "shear number", S, a measure of the stagger of the strands (*72*, *73*). Crystal structures of GFP-like proteins show that these proteins are characterized by an n of 11 and an S of >20, a mean slope of the strands with respect to the long axis of the protein (α) of 41°, and a mean radius of the barrel of approximately 12 Å. In contrast to the proteins studied in refs *72* and *73*, GFP-like proteins contain a central α-helix. However, the proposed condition for efficient side chain packing, and therefore low-energy β-barrels, $S = 2n$ (*73*), is fulfilled to good approximation. Therefore, inefficient side chain packing is unlikely to be the origin of the disturbed hydrogen bonding network.

Several indications underline the importance of dynamical processes around β-strand 7. First, according to molecular dynamics simulations, conformational fluctuations occur in the cleft between β-sheets 7 and 8, mainly connected to flipping of the Arg168 side chain (*71*) at least on a nanosecond time scale. Second, ^{19}F NMR studies on the cyan variant of GFP showed that His148 is likely to be involved in a slow exchange process (*25*). Finally, Haupts et al. (*29*) have speculated that conformational fluctuations are the origin of the pH sensitivity of the GFP chromophore (*29*). For example, mutations at positions 147, 149, 164−168, 202, and 220 (located in β-strands 7, 8, 10, and 11) have been shown to increase the pH sensitivity of the GFP chromophore (*74*). This effect is supposed to be caused by an increased conformational flexibility around the chromophore. Therefore, a dynamic process, e.g., an exchange between different backbone conformations, is most likely the origin of the increased hydrogen exchange rates which may also explain

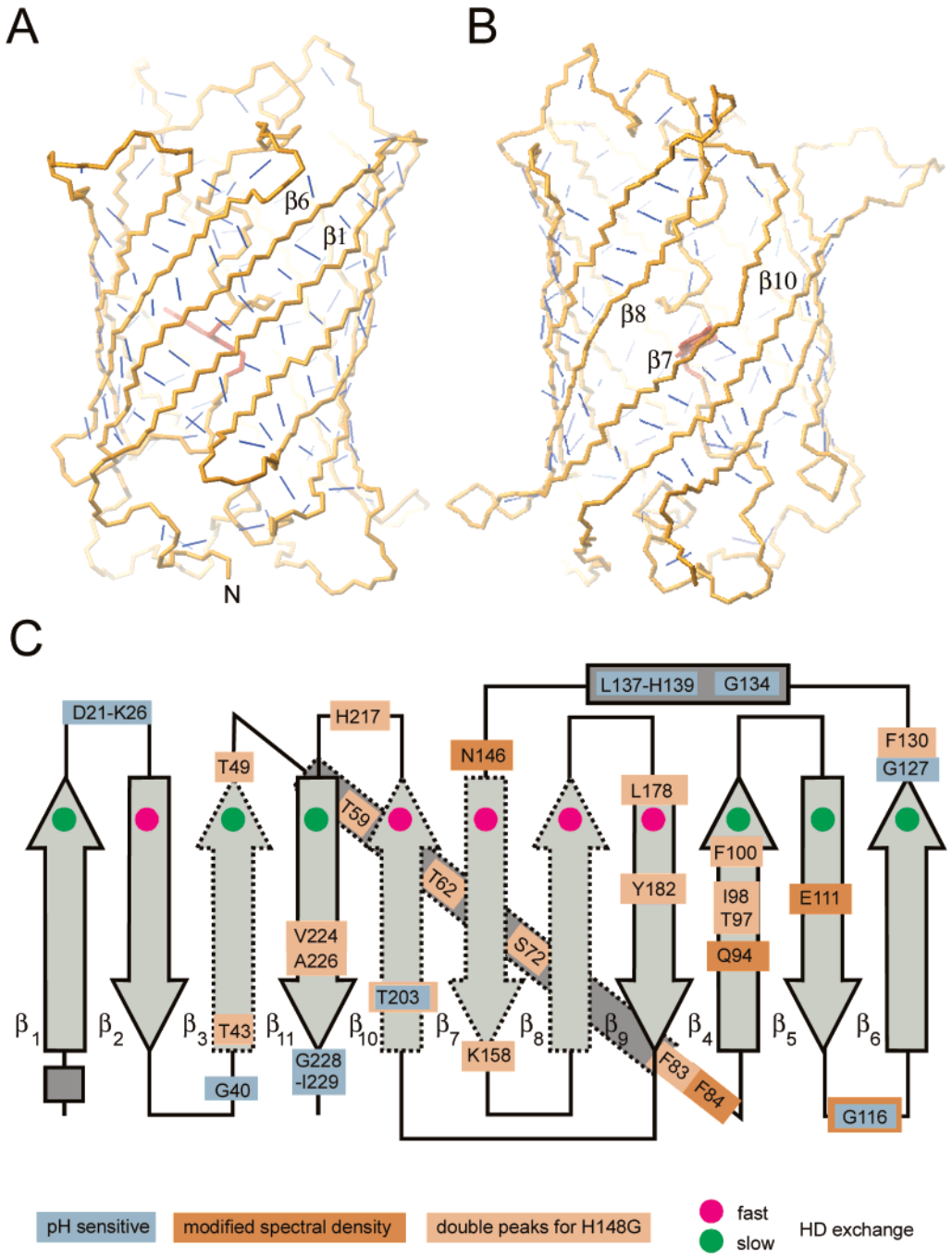

FIGURE 9: Hydrogen bonding network (blue lines) on opposite sides of the GFP β-barrel (A) and (B) based on the crystal structure coordinates from PBD entry 1b9c (*30*). These figures were created using MOLMOL (*80*). The observed dynamic properties of GFPuv are mapped on the GFP fold (C). β-Sheets and α-helices are drawn as arrows and boxes, respectively. Dotted arrows indicate β-sheets with incomplete resonance assignments.

the difficult resonance assignment in this part of the protein.

In summary, the observed H−D rates indicate a higher degree of conformational fluctuations that disturb the interstrand hydrogen bonding network around β-strand 7. NMR methods for directly assessing hydrogen bonds exist, e.g., via the $^{1}J_{NC'}$ coupling constants, but the high molecular weight and aggregation tendency of GFP preclude the practical usage of such sequences (*75, 76*).

From the point of view of fluorescence, the observed conformational flexibility is not optimal for a high quantum yield. For example, such motions may allow fluorescence quenchers such as oxygen to enter the β-barrel. In addition, the backbone flexibility may also affect the chromophore-stabilizing network and therefore increase the rate of photoisomerization. To further optimize the fluorescence properties of GFPs by reducing the conformational flexibility, clarification about whether this conformational flexibility is necessary for protein folding or if suitable mutations can reduce such structural instabilities is needed. However, since β-strand 7 is interrupted around residue 148 in most GFP structures and surprisingly also in the nidogen-1 structure where Tyr540 corresponds to His148, the presence of a predetermined breaking point at this point is suggested. Helms et al. (*71*) have speculated that the closure of the cleft between β-strands 7 and 8 is one of the last events in the formation of the β-barrel upon folding of the protein. It is

therefore more likely that the mentioned flexibility is an intrinsic property of the GFP fold that might result from its folding.

Effect of the Histidine 148 Substitution. To further investigate the relationship between the structural properties of β-strands 7, 8, and 10 and GFP function (i.e., fluorescence), histidine 148 located in β-sheet 7 was mutated to glycine. The most apparent difference between the optical properties of GFPuv His148Gly and those of native GFPuv is the strong reduction of absorption at 478 nm, termed band B arising from the anionic state of the chromophore. In addition, our results here show that this mutation leads to the appearance of allosteric slow exchange processes in the protein backbone. Therefore, this mutation destabilizes the overall structure of the protein, leading to either an increase in the amplitude of low-frequency motions or a shift in the time scale which makes the motions visible in the HSQC spectrum. It has been shown before that the mutation of histidine 148 to glycine in YFP causes a larger β-strand separation between the backbones of residues 148 and 168 (*77*). The side chain of Ile167 is relocated toward the space previously occupied by the imidazole ring. In GFP, β-strands 7 and 8 are connected by a hydrogen bond between His148 Nϵ and Arg168 N. In the wild-type crystal structure (*19*), Arg168 folds over His148. Therefore, removal of His148 is supposed to destabilize the protein barrel, leading to more pronounced conformational fluctuations. These fluctuations may propagate throughout the otherwise tightly bound β-strands and cause the observed allosteric effect. The effect observed in GFPuv His148Gly has to be distinguished from the slow exchange process observed in CFP (*25*) which takes place on a much shorter time scale ($\tau_{ex} = 1.3$ ms) compared to that of GFPuv His148Gly ($\tau_{ex} > 0.01-0.1$ s).

The most interesting question that arises from our observations is whether a mechanistic link can be drawn between structural dynamics derived from NMR data and optical properties. First of all, since light absorption takes place on the femtosecond time scale, much faster than any structural process in proteins, UV absorption spectra display only an instantaneous average of the immediate chromophore environment (*78*). Second, for the interpretation of fluorescence data, it is always necessary to infer the physiochemical behavior of the environment from measured photophysical parameters on the assumption that the photophysical responses are understood a priori, i.e., a plausible model of the chromophore and its environment is available (*79*). For GFP, a model of photophysics has been derived from crystal structures in combination with time-resolved fluorescence measurements (*2*, *13*). In the case of GFPuv His148Gly, the main question is whether the observed strong reduction in absorption of the anionic state B (whereas the fluorescence emission is nearly unchanged) is related to the structural inhomogeneity as seen in NMR spectra. The creation of the nonequilibrium excited I* state, which is supposed to give rise to the fluorescence emission, by deprotonation of the chromophore's phenolic oxygen seems to be quite unaffected by the His148Gly mutation. However, the anionic state's B $\rightarrow$ B* transition is significantly less prominent which may be attributed to a shifted ratio of neutral to anionic states in the chromophore's thermodynamic equilibrium. So, according to our hypothesis, the substitution of His148 with glycine and therefore removal of a major part of the internal hydrogen bonding network affects only the state of chromophore protonation in equilibrium. The access of solvent molecules through the structural fluctuations in the β-barrel alters the immediate chromophore environment but still allows a fast and effcient creation of the fluorescent state by chromophore deprotonation. Further studies including time-resolved fluorescence spectroscopy and NMR relaxation measurements of the involved side chains have to be conducted to unambiguously determine the pathways of proton transfer in this mutant.

CONCLUSIONS

A structure-based sequence alignment of several GFP-like proteins suggests an important role of Phe27, Leu60, and several glycine residues for the GFP fold. Furthermore, this study shows that GFPuv exists in a dynamic dimer−monomer equilibrium in solution at the high concentrations used for NMR spectroscopy. The β-barrel structure of GFPuv is rigid on the nanosecond to picosecond time scale with only the connecting turns being flexible on the microsecond to millisecond time scale. The His148Gly mutation leads to a slow exchange process between two conformations of the β-barrel which may influence the chromophore's equilibrium state.

ACKNOWLEDGMENT

We thank Dr. Helena Kovacs of Bruker BioSpin (Zurich, Switzerland) for recording the spectra on the Cryoprobe system.

SUPPORTING INFORMATION AVAILABLE

Figures illustrating 1D proton NMR spectra of GFPuv and EGFP, the pH titration, the H−D exchange experiment, and $^{1}H-^{15}N$ HSQC spectra of GFPuv and its His148Gly mutant. This material is available free of charge via the Internet at http://pubs.acs.org.

REFERENCES

1. Chalfie, M., Tu, Y., Euskirchen, G., Ward, W. W., and Prasher, D. C. (1994) *Science 263*, 802−805.
2. Tsien, R. Y. (1998) *Annu. Rev. Biochem. 67*, 509−544.
3. Chattoraj, M., King, B. A., Bublitz, G. U., and Boxer, S. G. (1996) *Proc. Natl. Acad. Sci. U.S.A. 93*, 8362−8367.
4. Lossau, H., Kummer, A., Heinnecke, R., Pöllinger-Dammer, F., Kompa, C., Bieser, G., Jonsson, T., Silvia, C., Yang, M., Youvan, D., and Michel-Beyerle, M. E. (1996) *Chem. Phys. 213*, 1−16.
5. Brejc, K., Sixma, T. K., Kitts, P. A., Kain, S. R., Tsien, R. Y., Ormo, M., and Remington, S. J. (1997) *Proc. Natl. Acad. Sci. U.S.A. 94*, 2306−2311.
6. Dickson, R., Cubitt, A., Tsien, R., and Woerner, W. (1997) *Nature 388*, 355−358.
7. Garcia-Parajo, M., Segers-Nolten, G., Veerman, J., Greve, J., and von Hulst, N. (2000) *Proc. Natl. Acad. Sci. U.S.A. 97*, 7237−7242.
8. Zumbusch, A., and Jung, G. (2000) *Single Mol. 4*, 261−270.
9. Harvey, E. N. (1921) *Biol. Bull. (Woods Hole, Mass.) 41*, 280−287.
10. Shimomura, O., and Johnson, F. H. (1978) *Methods Enzymol. 57*, 271−291.
11. Inouye, S., Noguchi, M., Sakaki, Y., Takagi, T., Iwanaga, S., Miyata, T., and Tsuji, F. I. (1985) *Proc. Natl. Acad. Sci. U.S.A. 82*, 3154−3158.
12. Charbonneau, H., Walsh, K. A., McCann, R. O., Prendergast, F. G., Cormier, M. J., and Vanaman, T. C. (1985) *Biochemistry 24*, 6762−6771.
13. Prendergast, F. (1999) *Methods Cell Biol. 58*, 1−18.

14. Förster, T. (1950) *Z. Elektrochem. 54*, 42−46.
15. van Thor, J. J., Pierik, A. J., Nugteren-Roodzant, I., Xie, A., and Hellingwerf, K. J. (1998) *Biochemistry 37*, 16915−16921.
16. van Thor, J. J., Gensch, T., Hellingwerf, K. J., and Johnson, L. N. (2002) *Nat. Struct. Biol. 9*, 37−41.
17. Labas, Y. A., Gurskaya, N. G., Yanushevich, Y. G., Fradkov, A. F., Lukyanov, K. A., and Matz, M. V. (2002) *Proc. Natl. Acad. Sci. U.S.A. 99*, 4256−4261.
18. Ormoe, M., Cubitt, A. B., Kallio, K., Gross, L. A., Tsien, R. Y., and Remington, S. J. (1996) *Science 273*, 1392−1395.
19. Yang, F., Moss, L. G., and Phillips, G. N., Jr. (1996) *Nat. Biotechnol. 14*, 1246−1251.
20. Striker, G., Subramaniam, V., Seidel, C. A. M., and Volkmer, A. (1999) *J. Phys. Chem. B 103*, 8612−8617.
21. Niwa, H., Inouye, S., Hirano, T., Matsuno, T., Kojima, S., Kubota, M., Ohashi, M., and Tsuji, F. I. (1996) *Proc. Natl. Acad. Sci. U.S.A. 93*, 13617−13622.
22. Bell, A. F., He, X., Wachter, R. M., and Tonge, P. J. (2000) *Biochemistry 39*, 4423−4431.
23. Ward, W. W. (1981) in *Bioluminescence and Chemiluminescence: Basic Chemistry and Analytical Applications* (DeLuca, M. A., and McElroy, W. D., Eds.) pp 235−242, Academic Press, New York.
24. Kummer, A. D., Wiehler, J., Rehaber, H., Kompa, C., Steipe, B., and Michel-Beyerle, M. E. (2000) *J. Phys. Chem. B 104*, 4791−4798.
25. Seifert, M. H. J., Ksiazek, D., Azim, M. K., Smialowski, P., Budisa, N., and Holak, T. A. (2002) *J. Am. Chem. Soc. 124*, 7932−7942.
26. Spyracopoulos, L., and Sykes, B. D. (2001) *Curr. Opin. Struct. Biol. 11*, 555−559.
27. Kay, L. E. (1998) *Nat. Struct. Biol.* (NMR Supp.), 513−517.
28. Dempsey, C. E. (2001) *Prog. Nucl. Magn. Reson. Spectrosc. 39*, 135−170.
29. Haupts, U., Maiti, S., Schwille, P., and Webb, W. W. (1998) *Proc. Natl. Acad. Sci. U.S.A. 95*, 13573−13578.
30. Battistutta, R., Negro, A., and Zanotti, G. (2000) *Proteins: Struct., Funct., Genet. 41*, 429−437.
31. Crameri, A., Whitehorn, E. A., Tate, E., and Stemmer, W. P. (1996) *Nat. Biotechnol. 14*, 315−319.
32. Hopf, M., Göhring, W., Ries, A., Timpl, R., and Hohenester, E. (2001) *Nat. Struct. Biol. 8*, 634−640.
33. Kummer, A. D., Kompa, C., Lossau, H., Pöllinger-Dammer, F., Michel-Beyerle, M. E., Silva, C., Bylina, E., Coleman, W., Yang, M., and Youvan, D. (1998) *Chem. Phys. 237*, 183−193.
34. Bulina, M. E., Chudakov, D. M., Mudrik, N. N., and Lukyanov, K. A. (2002) *BMC Biochem. 3*, 7.
35. Holm, L., and Sander, C. (1996) *Science 273*, 595−602.
36. Wall, M. A., Socolich, M., and Ranganathan, R. (2000) *Nat. Struct. Biol. 7*, 1133−1138.
37. Georgescu, J. (2000) Ph.D. Thesis, Faculty of Chemistry, TU Munich, Munich, Germany.
38. Georgescu, J., Ksiazek, D., Seifert, M. H. J., Rehm, T., Steipe, B., Holak, T. A., and Reuter, W. (2003) manuscript in preparation.
39. Cavanagh, J., Fairbrother, W. J., Palmer, A. G., III, and Skelton, N. J. (1996) *Protein NMR Spectroscopy: Principles and Practice*, Academic Press, San Diego.
40. Salzmann, M., Pervushin, K., Wider, G., Senn, H., and Wüthrich, K. (1998) *Proc. Natl. Acad. Sci. U.S.A. 95*, 13585−13590.
41. Mori, S., Abeygunawardana, C., Johnson, M. O., and van Zijl, P. C. (1995) *J. Magn. Reson., Ser. B 108*, 94−98.
42. Goddard, T. D., and Kneller, D. G. (2002) *SPARKY 3*, University of California, San Francisco.
43. Cieslar, C., Holak, T. A., and Oschkinat, H. (1990) *J. Magn. Reson. 87*, 400−407.
44. Dingley, A. J., Mackay, J. P., Chapman, B. E., Morris, M. B., Kuchel, P. W., Hambly, B. D., and King, G. F. (1995) *J. Biomol. NMR 6*, 321−328.
45. Sklenar, V., Piotto, M., Leppik, R., and Saudek, V. (1993) *J. Magn. Reson. 102*, 241−245.
46. Seifert, M. H. J. (2002) Ph.D. Thesis, Faculty of Chemistry, TU Munich, Munich, Germany.
47. Cantor, C., and Schimmel, P. R. (1980) *Biophysical Chemistry Part II*: *Techniques for the study of biological structure and function*, W. H. Freeman and Co., San Francisco.
48. Skelton, N. J., Palmer, A. G., III, Akke, M., Kördel, J., Rance, M., and Chazin, W. J. (1993) *J. Magn. Reson., Ser. B 102*, 253−264.
49. Zweckstetter, M., and Holak, T. A. (1998) *J. Magn. Reson., Ser. B 133*, 134−147.
50. Neuhaus, D., and Williamson, M. P. (2000) *The Nuclear Overhauser Effect in Structural and Conformational Analysis*, 2nd ed., Wiley-VCH, New York.
51. Tjandra, N., Szabo, A., and Bax, A. (1996) *J. Am. Chem. Soc. 118*, 6986−6991.
52. Markley, J. L., Horsley, W. J., and Klein, M. P. (1971) *J. Chem. Phys. 55*, 3604−3605.
53. Sklenar, V., Torchia, D., and Bax, A. (1987) *J. Magn. Reson. 73*, 375−379.
54. Abragam, A. (1961) *Principles of nuclear magnetism*, Clarendon Press, Oxford, U.K.
55. Peng, J. W., and Wagner, G. (1992) *J. Magn. Reson., Ser. B 98*, 308−332.
56. Peng, J. W., and Wagner, G. (1992) *Biochemistry 31*, 8571−8586.
57. Lefévre, J.-F., Dayie, K. T., Peng, J. W., and Wagner, G. (1996) *Biochemistry 35*, 2674−2686.
58. Clore, G. M., Driscoll, P. C., Wingfield, P. T., and Gronenborn, A. M. (1990) *Biochemistry 29*, 7387−7401.
59. Fushman, D., Weisemann, R., Thüring, H., and Rüterjans, H. (1994) *J. Biomol. NMR 4*, 61−78.
60. Philips, G. N. (1998) in *Green Fluorescent Protein* (Chalfie, M., and Kain, S., Eds.) Wiley-Liss, New York.
61. Fushman, D., and Cowburn, D. (1998) *J. Am. Chem. Soc. 120*, 7109−7110.
62. Lipari, G., and Szabo, A. (1982) *J. Am. Chem. Soc. 104*, 4546−4570.
63. Mok, Y. K., Elisseeva, E. L., Davidson, A. R., and Forman-Kay, J. D. (2001) *J. Mol. Biol. 307*, 913−928.
64. Cheng, Z. Q., and McFadden, B. A. (1998) *Protein Eng. 11*, 457−465.
65. Gardner, K. H., Zhang, X. C., Gehring, K., and Kay, L. E. (1998) *J. Am. Chem. Soc. 120*, 11738−11748.
66. Fukuda, H., Arai, M., and Kuwajima, K. (2000) *Biochemistry 39*, 12025−12032.
67. Zacharias, D. A., Violin, J. D., Newton, A. C., and Tsien, R. Y. (2002) *Science 296*, 913−916.
68. Campbell, R. E., Tour, O., Palmer, A. E., Steinbach, P. A., Baird, G. S., Zacharias, D. A., and Tsien, R. Y. (2002) *Proc. Natl. Acad. Sci. U.S.A. 99*, 7877−7882.
69. Fernandez, C., Hilty, C., Bonjour, S., Adeishvili, K., Pervushin, K., and Wüthrich, K. (2001) *FEBS Lett. 504*, 173−178.
70. Schulz, G. E. (2000) *Curr. Opin. Struct. Biol. 10*, 443−447.
71. Helms, V., Straatsma, T. P., and McCammon, J. A. (1999) *J. Phys. Chem. 103*, 3263−3269.
72. McLachlan, A. D. (1979) *J. Mol. Biol. 128*, 49−79.
73. Murzin, A. G., Lesk, A. M., and Chothia, C. (1994) *J. Mol. Biol. 236*, 1369−1400.
74. Miesenböck, G., De Angelis, D. A., and Rothman, J. E. (1998) *Nature 394*, 192−195.
75. Juranic, N., Ilich, P. K., and Macura, S. (1995) *J. Am. Chem. Soc. 117*, 405−410.
76. Juranic, N., Likic, V. A., Prendergast, F. G., and Macura, S. (1996) *J. Am. Chem. Soc. 118*, 7859−7860.
77. Wachter, R. M., Elsiger, M. A., Kallio, K., Hanson, G. T., and Remington, S. J. (1998) *Structure 6*, 1267−1277.
78. Lakowicz, J. R. (1999) *Principles of Fluorescence Spectroscopy*, 2nd ed., Kluwer Academic, New York.
79. Moncrieffe, M. C., Juranic, N., Kemple, M. D., Potter, J. D., Macura, S., and Prendergast, F. G. (2000) *J. Mol. Biol. 297*, 147−163.
80. Koradi, R., Billeter, M., and Wüthrich, K. (1996) *J. Mol. Graphics 14*, 51−55.

BI026481B